Published in final edited form as:
Neuron. 2011 December 8; 72(5): 721–733. doi:10.1016/j.neuron.2011.10.028.

Recombinase-driver rat lines: tools, techniques, and optogenetic application to dopamine-mediated reinforcement

Ilana B. Witten[1,2,*,¶], **Elizabeth E. Steinberg**[3,4,*], **Soo Yeun Lee**[1,5], **Thomas J. Davidson**[1], **Kelly A. Zalocusky**[1,13], **Matthew Brodsky**[1,6], **Ofer Yizhar**[1,7], **Saemi L. Cho**[3], **Shiaoching Gong**[8], **Charu Ramakrishnan**[1], **Garret D. Stuber**[9], **Kay M. Tye**[1,10], **Patricia H. Janak**[3,4,¶], and **Karl Deisseroth**[1,5,11,12,13,¶]

[1]Department of Bioengineering, Stanford University, Stanford, CA 94305, USA

[2]Princeton Neuroscience Institute & Department of Psychology, Princeton, NJ 08544, USA

[3]Ernest Gallo Clinic and Research Center, UCSF, Emeryville, CA 94608, USA

[4]Neuroscience Graduate Program, UCSF, San Francisco, CA 94158, USA

[5]CNC Program, Stanford University, Stanford, CA 94305, USA

[6]Graduate Program in Neurobiology and Behavior, University of Washington, Seattle, WA 98195, USA

[7]Department of Neurobiology, Weizmann Institute, Rehovot 76100, Israel

[8]The GENSAT Project, The Rockefeller University, New York, NY 10065, USA

[9]Departments of Psychiatry & Cell and Molecular Physiology, UNC Neuroscience Center, University of North Carolina, Chapel Hill, NC 27599 USA

[10]Picower Institute of Learning and Memory, Department of Brain and Cognitive Sciences, MIT, Cambridge MA 02139, USA

[11]Department of Psychiatry, Stanford University, Stanford, CA 94305, USA

[12]HHMI, Stanford, CA 94305, USA

[13]Neuroscience Graduate Program, Stanford University, Stanford CA, 94305

Summary

Currently there is no general approach for achieving specific optogenetic control of genetically-defined cell types in rats, which provide a powerful experimental system for numerous established neurophysiological and behavioral paradigms. To overcome this challenge we have generated genetically-restricted recombinase-driver rat lines suitable for driving gene expression in specific cell-types, expressing Cre recombinase under control of large genomic regulatory regions (200–300 Kb). Multiple tyrosine hydroxylase *(Th)::Cre* and choline acetyltransferase *(Chat)::Cre* lines were produced that exhibited specific opsin expression in targeted cell-types. We additionally developed methods for utilizing optogenetic tools in freely-moving rats, and leveraged these technologies to clarify the causal relationship between dopamine (DA) neuron firing and positive reinforcement, observing that optical stimulation of DA neurons in the ventral tegmental area (VTA) of *Th::Cre* rats is sufficient to support vigorous intracranial self-stimulation (ICSS). These

[¶]To whom correspondence should be addressed: Karl Deisseroth, M.D., Ph.D., deissero@stanford.edu, +1.650.736.4325. Patricia H. Janak, Ph.D., pjanak@gallo.ucsf.edu, +1.510.985.3880. Ilana B. Witten, Ph.D., iwitten@princeton.edu, +1.650.804.9261.
[*]equal contribution

studies complement existing targeting approaches by extending generalizability of optogenetics to traditionally non-genetically-tractable but vital animal models.

Introduction

While genetically-modified mice have enabled substantial advances in neuroscience and have made possible new approaches for circuit analysis with optogenetics (Tsai et al., 2009; Gradinaru et al., 2009; Lobo et al., 2010; Kravitz et al., 2010; Witten et al., 2010; Tye et al., 2011), a generalizable approach for optogenetic targeting of genetically-defined cell types in rats has proven to be elusive. This technological limitation is particularly important to address given that the substantial and flexible behavioral repertoire of rats makes these animals the preferred rodent model in many fields of neuroscience experimentation, and a wide variety of behavioral tasks have been optimized for this species (Bari et al., 2008; Chudasama and Robbins, 2004; Uchida and Mainen, 2003; Otazu et al., 2009; Pontecorvo et al., 1996; Vanderschuren and Everitt, 2004; Phillips et al., 2003; Pedersen et al., 1982). Furthermore, rats represent an essential system for *in vivo* electrophysiology, with dimensions that enable accommodation of the substantial numbers of electrodes required to obtain simultaneous data from large neuronal populations (Wilson and McNaughton, 1993; Royer et al., 2010; Buzsàki et al., 1989; Gutierrez et al., 2010; Colgin et al., 2009; Jog et al., 2002; Berke et al., 2009). Therefore, the ability to utilize population-selective genetically-targeted optogenetic tools in the rat would be a valuable technical advance.

Most efforts to target genetically-defined neurons in rats have relied on viral strategies, but given the paucity of compact and well-characterized promoters, this approach has only rarely led to highly specific targeting (Lee et al., 2010; Lawlor et al., 2009; Nathanson et al., 2009). Alternatively, transgenic rat lines can be generated to enable use of specific larger promoter-enhancer regions (Filipiak and Saunders, 2006), but for expression of opsins in the brain this approach suffers from two serious limitations. First, this method is low-throughput and not well suited for keeping pace with the rapidly advancing opsin toolbox (requiring specific design, line generation, multi-generational breeding, and testing of each individual rat line for a particular opsin gene). Second, this approach is inconsistent with straightforward optogenetic control of single or multiple spatially distinct populations; in fact, a breakdown in specificity for control of cells or projections within a particular illuminated brain region arises because opsins traffic efficiently down axons (Gradinaru et al., 2010) and incoming afferents from other brain regions that are photosensitive will confound experiments by exhibiting optical sensitivity alongside local cell populations. For example, in a rat line expressing opsins in all catecholamine neurons, illumination of the ventral tegmental area (VTA) would activate both dopamine (DA) cell bodies in the VTA and noradrenergic projections to the VTA originating from cells in the locus coeruleus.

Here, we explore an alternative approach addressing all of the above fundamental limitations, instead generating a panel of the first characterized and specific transgenic recombinase-driver rat lines, with regulatory information contained in 200–300 Kb of DNA upstream and downstream of the target genes (an approach that has achieved considerable success in mice; Gong et al., 2007). In these rats, large amounts of regulatory information is packaged in bacterial artificial chromosomes (BACs), with packaging capability that can accommodate regulatory sequences dispersed across large regions of the genome. We then apply these resources in combination with a panel of novel rat-specific optogenetic behavioral approaches and spatially-specific injection of Cre-dependent opsin-expressing viral vectors, to explore the causal relationship between DA neuron firing and positive reinforcement during optical intracranial self-stimulation (ICSS) in freely moving rats.

Over the course of the last half-century, electrical ICSS has emerged as a powerful approach to identify brain areas that serve as positive reinforcement sites (Olds and Milner, 1954; Olds, 1963; Corbett and Wise, 1980), and the bulk of the relevant experiments have been conducted in rats. An extensive literature suggests that DA neurons play an important role in electrical ICSS, as altering levels of DA or lesioning DA neurons dramatically affects ICSS thresholds (Fibiger et al., 1987; German and Bowden, 1974; Fouriezos and Wise, 1976; Mogenson et al., 1979; Wise and Rompré, 1989) and effective sites for ICSS, including the medial forebrain bundle, closely parallel the anatomical location of DA neurons or their broad projections (Corbett and Wise, 1980). However, several studies have suggested that powerful ICSS sites may have a non-dopaminergic component, or perhaps not even require DA neurons at all. Robust ICSS has been demonstrated behaviorally without metabolic activation of major dopaminergic projection targets (Gallistel et al., 1985), and rats with near-complete lesions of the DA system show reduced but still significant ICSS behavior (Fibiger et al., 1987). Additionally, the electrophysiological properties of axons thought to be necessary for sustaining ICSS were shown to be inconsistent with the conduction velocity of DA axons (Bielajew and Shizgal, 1986). Further, studies employing *in vivo* voltammetry during ICSS have found that DA release in the nucleus accumbens (NAc), a major efferent target of DA neurons, is only rarely observed in well-trained animals (Owesson-White et al., 2008; Garris et al., 1999). Finally, a recent optogenetic study in mice found that DA neuron stimulation by itself was not sufficient for the acquisition of ICSS (Adamantidis et al, 2011).

The challenge in linking DA neuron activation to ICSS may be rooted in the complexity and heterogeneity of the rat VTA, coupled with ambiguities inherent to electrical stimulation. Less than 60% of neurons in the rat VTA are dopaminergic (Margolis et al., 2006; Fields et al., 2007; Nair-Roberts et al. 2008; Swanson, 1982). The sizeable population of GABAergic and to a lesser extent glutamatergic neurons that constitute the remainder send extensive efferent projections both within and outside of the VTA (Dobi et al., 2010; Yamaguchi et al., 2011). An additional concern arises from recent imaging experiments demonstrating that electrical stimulation activates a sparse and scattered neural population with a spatial distribution that is difficult to predict (Histed et al., 2009). This issue is particularly significant given the wide array of brain areas that support electrical ICSS (Wise, 1996; German and Bowden, 1974; Olds and Olds, 1963). Electrical stimulation of the VTA therefore undoubtedly activates a complex and heterogeneous circuitry; to circumvent this issue we applied one of the novel recombinase driver rat lines developed and reported here to test the hypotheses that direct activation of VTA DA neurons will be sufficient to 1) acquire and 2) sustain ICSS in freely-moving rats.

Results

Specific targeting of dopaminergic and noradrenergic neurons in Th::Cre rats

We first generated multiple BAC transgenic rat lines expressing Cre recombinase in tyrosine hydroxylase (TH) neurons (Experimental Procedures), and tested the specificity and potency of these lines for potential optogenetic experiments (Figs. 1–3). Injection of a Cre-dependent virus in dopaminergic (VTA or substantia nigra pars compacta, SN) or noradrenergic (locus coeruleus, LC) structures in *Th::Cre* rat lines resulted in highly specific channel rhodopsin-2 (ChR2) expression in catecholamine neurons (Fig. 1A–D). In the case of the VTA and SN injection, opsin expression was confined to TH+ cell bodies and processes (Fig. 1A–C), and to projections of these cells within known target structures (e.g. ventral and dorsal striatum, Fig. 1C, bottom). Similarly, with the LC as an injection target, opsin expression was confined to the TH+ LC cell bodies and their processes; Fig. 1D). Additionally, to confirm that the VTA and LC could be targeted independently in this rat line (a potential concern because both areas express TH and therefore Cre), virus was injected in the VTA and lack of expression was demonstrated in the LC (Fig. S1).

Importantly, *Th::Cre* sublines from different founders varied quantitatively in specificity and strength of expression (Fig. 1A). The offspring of founder 3 (line 3.1, 3.2, and 3.5) were used in all experiments in this paper, chosen for the highest specificity. For example, in the VTA of line 3.5, 99+/−1% of neurons that expressed ChR2-YFP also expressed TH (a measure of specificity), while 61+/−4% of neurons that expressed TH also expressed ChR2-YFP (a measure of the proportion of targeted neurons that expressed the transgene). In the SN of line 3.1 84+/−4% of neurons that expressed ChR2-YFP also expressed TH, while 77+/−5% of neurons that expressed TH also expressed ChR2-YFP. In the LC of line 3.1, 97+/−1% of neurons that expressed ChR2-YFP also expressed TH, while 72+/−6% of neurons that expressed TH also expressed ChR2-YFP (*n*=122 for VTA, *n*=86 for SN, *n*=63 for LC, where *n* refers to counted cells; Fig. 1A). To further characterize these lines, we quantified the copy number of *Cre* in *Th::Cre* rats with digital PCR (Supplemental Experimental Procedures). Across multiple sublines (*Th::Cre* 3.1, 3.5 and 4.4), we observed a single copy-number of *Cre* in the genome (Table S1).

We performed a systematic *in vitro* electrophysiological study of the cellular and optogenetic properties of ChR2-YFP-expressing VTA neurons in *Th::Cre*+ rats, along with a comparison of the same properties of neurons in *Th::Cre*+ littermates injected with a control virus that expressed only YFP. Figure 2A shows a sample trace from a ChR2-expressing *Th::Cre* neuron in response to current injection steps, demonstrating the classical "sag" response induced by the hyperpolarizing pulse, the result of a hyperpolarization-activated cation current (I_h) that is present in many TH+ VTA neurons (Margolis et al., 2006; Lammel et al., 2008, 2011; Neuhoff et al., 2002). Given that the VTA TH+ neurons are heterogeneous and do not all express a prominent I_h (Lammel 2008, 2011), in addition to analyzing light-responses and intrinsic properties of neurons with a prominent I_h current ($I_{h/large}$ neurons), we have also included in this analysis cells without a prominent I_h ($I_{h/small}$ neurons), in either case comparing the properties of neurons that express ChR2-YFP to neurons that express YFP only.

Continuous blue light elicited large inward currents (peak photocurrent: −2950 ± 1574 pA for $I_{h/large}$ neurons, steady-state photocurrent: −756.5 ± 225.5 pA; n=7 $I_{h/large}$ neurons, Fig. 2B), and optical stimulation trains produced neural responses that were similar to those evoked by electrical stimulation in both ChR2-expressing or YFP-only expressing neurons (Fig. 2C for pulse trains, Fig. S2D for individual waveforms); notably, the amplitude of both optically- and electrically-evoked spike trains attenuated during the course of the pulse train. *Th::Cre* ChR2-expressing neurons reliably responded to light-induced spike trains over a range of frequencies from 5–40Hz (Fig. 2D for $I_{h/large}$ neurons, Fig. S2B for $I_{h/small}$ neurons). Multiple spikes in response to a single light pulse were never observed during the presentation of pulse trains under these expression, illumination, and opsin (ChR2) conditions. We also confirmed that light stimulation at various frequencies (5 to 40 Hz) failed to evoke neural responses in YFP-only expressing neurons (Fig. S2C).

Additionally, we compared the intrinsic properties of ChR2-YFP and YFP-only expressing neurons from *Th::Cre* rats to control for the possibility that these properties may have been altered by ChR2 expression. We found that expression of ChR2 did not significantly alter the initial resting membrane potential (−42.6 ± 1.2 MΩ for ChR2 $I_{h/large}$ cells vs. −45.6 ± 0.5 MΩ for YFP $I_{h/large}$ cells; −45.4 ± 0.8 for ChR2 $I_{h/small}$ cells vs. −44.1 ± 5.6 YFP $I_{h/small}$ cells), magnitude of the I_h current (486.0 ± 161.1 pA for ChR2 $I_{h/large}$ cells vs. 507.2 ± 295.5 MΩ for YFP $I_{h/large}$ cells; 78.5 ± 36.0 pA for ChR2 $I_{h/small}$ cells vs. 52.6 ± 21.8 pA for YFP $I_{h/small}$ cells), input resistance (502.0 ± 72.6 MΩ for ChR2 $I_{h/large}$ cells vs. 616.3 ± 41.2 MΩ for YFP $I_{h/large}$ cells; 474.1 ± 56.6 MΩ for ChR2 $I_{h/small}$ cells vs. 465.1 ± 109.4 MΩ for YFP $I_{h/small}$ cells), and action potential threshold (−27.6 ± 12.9 mV for ChR2 $I_{h/large}$ cells vs. −30.0 ± 4.35 MΩ for YFP $I_{h/large}$ cells; −25.4 ± 7.4 mV for ChR2 $I_{h/small}$ cells vs. −27.0 ±

7.1 MΩ for YFP $I_{h/small}$ cells) as compared to YFP-only expressing neurons (Fig. S2A, n=7 for ChR2 $I_{h/large}$ cells, n=3 for YFP $I_{h/large}$ cells, n=4 for ChR2 $I_{h/small}$ cells, n=5 for YFP $I_{h/small}$ cells, p>0.05 for all comparisons, two-tailed t-test).

To complement the *in vitro* recordings and more fully characterize these new optogenetic tools, we validated tool functionality with electrophysiology *in vivo* as well. Optical stimulation of ChR2-expressing TH neurons resulted in reliable light-evoked neural activity *in vivo* assessed with optrodes; in particular, the targeted population was able to follow 20 Hz stimulation with a steady-state response level that was stable after 10 light pulses, and extending to at least 100 pulses (Fig. 2E).

Next, to confirm that light-evoked neural activity resulted in neurotransmitter release, we used fast-scan cyclic voltammetry to measure DA release in acute brain slices of the NAc of *Th::Cre* rats that had been injected in the VTA with a Cre-dependent ChR2-expressing virus (Fig. 3). 1 second of 20 Hz optical stimulation resulted in phasic transients with the characteristic DA current/voltage relationship (example site, Fig. 3A); across the population, mean amplitude of the transient was 0.33+/− 0.1 μM (*n*=17 recording sites). The amplitude of the NAc DA transient increased monotonically but not linearly with the number of 20 Hz stimulation pulses; this quantitative relationship is illustrated in Figure 3B. Light-evoked phasic DA release was TTX-dependent (Fig. 3C), implicating presynaptic activation of voltage-gated Na^+ channels in optically-evoked DA release.

Specific targeting of cholinergic neurons in Chat::Cre rats

A separate set of Cre driver rat lines was also generated, in this case leading to specific optogenetic targeting of cholinergic neurons and demonstrating the versatility of this approach (Fig. 4). In the medial septum of *Chat::Cre* line 5.2, 92+/−2% of neurons that expressed YFP also expressed ChAT, and 51+/−4% of neurons that expressed ChAT also expressed YFP (*n*=118); in the nucleus basalis, 98+/−1% of neurons that expressed YFP also expressed ChAT, and 88+/−3% of neurons that expressed ChAT also expressed YFP (*n*=173 neurons); in the NAc, 97+/−3% of neurons that expressed YFP also expressed ChAT, and 90+/−5% of neurons that expressed ChAT also expressed YFP (*n*=40 neurons) (Fig. 4A,B). A quantification of copy number in the *Chat::Cre* lines revealed an estimated copy number of 6 (Table S1), which may contribute to the high proportion of ChAT neurons that expressed YFP in the nucleus basalis and the NAc.

Since direct optrode recording of ChAT neurons *in vivo* is much more challenging due to population sparsity (in contrast to the relatively abundant TH neurons in the VTA; Fig 2E), we confirmed light-evoked neural activation with acute slice patch-clamp recordings of neurons in the nucleus basalis that expressed ChR2-YFP (Fig. 4C,D). This approach revealed that optical stimulation of ChAT cells led to large inward currents (>500 pA) as well as robust light-evoked action potentials across a broad frequency range (5–40Hz Fig. 4E). Moreover, we were able to employ optrode recordings *in vivo* to assess the effect of the directly activated ChAT cells on surrounding circuitry; when these cells were optically stimulated *in vivo*, we observed potent inhibition of spontaneous spiking in surrounding cells of the nucleus basalis, revealing not only light-driven spiking but also potent light-driven influences on neural circuit function in this Cre driver rat line (Fig. 4F).

Methods for Optogenetic Stimulation in Freely-Moving Rats

In order to capitalize on these new reagents, we developed a system for optogenetic stimulation in freely behaving rats (Fig. 5). The essential components of this system are (1) an implantable optical fiber to reduce fiber breakages that result from repeatedly connecting to a light source over multiple behavioral sessions, (2) a secure connection between the

implanted fiber and optical cable, (3) a protective spring encasing the optical patch cable to improve durability, (4) a counterbalanced lever arm to reduce tension associated with the attached cable, and (5) an optical commutator to allow the optical cable attached to the rat to rotate freely during behavioral sessions. The design and use of these rat-optimized optogenetic tools are described in the Experimental Procedures.

Application to Dopamine-Mediated Positive Reinforcement

Finally, we applied this technology to map quantitative relationships between activation of VTA DA neurons in rats and self-stimulation behavior. *Th::Cre+* rats and their wild-type littermates received identical injections of Cre-dependent ChR2 virus in the VTA, as well as optical fiber implants targeted dorsal to this structure (Fig. 6A; see Figure S3 for placement summary and fluorescence images). All rats were given the opportunity to respond freely at two identical nosepoke ports. A response at the active port resulted in a 1 second train of light pulses (20 Hz, 20 pulses, 5 ms pulse duration) delivered on a fixed-ratio 1 (FR1) schedule, while responses at the inactive port were without consequence. *Th::Cre+* rats made significantly more responses at the active port relative to the inactive port on all 4 days of training (Fig. 6B, 2-tailed Wilcoxon signed rank test with Bonferroni correction, $p<0.05$ on days 1–4; see also Fig. 6C for cumulative active nosepoke responding across all days of training for a representative rat) indicating rapid acquisition of DA ICSS. By the third and fourth training day, *Th::Cre+* rats performed more than 4,000 nosepokes on average at the active port, compared to less than 100 at the inactive port (Fig. 6B). Variability in the vigor of responding between subjects (Fig. 6D) could explained by differences in the strength of virus expression directly beneath the implanted optical fiber tip (t-test, $p<0.05$, $r^2=0.55$; see Fig. S3A–C for placement summary and fluorescence quantification). Additionally, *Th::Cre−* rats made significantly fewer nosepokes at the active port than *Th::Cre+* rats on all 4 days (2-tailed Mann-Whitney test with Bonferroni correction, $p<0.05$ on day 1, $p<0.005$ on days 2–4). Notably, responding of *Th::Cre−* rats at the active port was indistinguishable from responding at the inactive port (2-tailed Wilcoxon signed rank test with Bonferroni correction; $p>0.05$), indicating that active port responses in *Th::Cre−* rats were not altered by optical stimulation.

We then systematically varied the duration of optical stimulation that was provided for each single active nosepoke response in order to investigate the relationship between the magnitude of DA neuron activation and the vigor of behavioral responding (“duration-response test”). We chose to vary stimulation duration, having already established that altering this parameter results in corresponding changes in evoked DA transients *in vitro* (Fig. 3B). Further, varying this parameter allowed us to confirm that later spikes in a stimulation train are still propagated faithfully to generate DA release in behaving rat (in agreement with our *in vitro* confirmation, Fig. 3B). The rate of responding of *Th::Cre+* rats at the active nosepoke port depended powerfully on the duration of stimulation received (Fig. 6E, Kruskal-Wallis Test, $p<0.0001$). Response rate increased more than threefold as the duration of the stimulation train increased from 5 ms to 1 second, and saturated for durations above 1 second. This saturation could not be explained by a ceiling effect on the number of reinforcers that could be earned, since even for the longest stimulation train durations, rats earned on average less than 50% of the possible available optical stimulation trains (Fig. 6E, inset).

We further applied two classical behavioral tests to confirm that rats were responding to obtain response-contingent optical stimulation, rather than showing non-specific increases in arousal and activity subsequent to DA neuron activation. First, we tested the effect of discontinuing stimulation during the middle of a self-stimulation session. Rats were allowed to respond over 30 min for 1-second stimulation trains (20 Hz, 20 pulses, 5 ms pulse duration; “maintenance”). Subsequently, stimulation was discontinued and responses at the

active port had no effect ("extinction"). After a further 30 minutes had elapsed, brief "priming" stimulation trains were delivered to indicate to the rat that stimulation was once again available ("reacquisition"). We found that *Th::Cre+* rats rapidly extinguished and then reacquired responding for DA ICSS, performing significantly fewer active nosepokes during extinction as compared to both maintenance and reacquisition (2-tailed Wilcoxon signed rank test; $p<0.01$ for maintenance vs extinction, $p<0.05$ for extinction vs reacquisition, Fig. 6F,G). The extinction of active responding was rapid; within 5 minutes after extinction onset, rats had decreased their average rate of responding at the active nosepoke to less than 10% of the rate sustained during maintenance. Importantly, by the last 5 minutes of the extinction phase *Th::Cre+* rats no longer responded preferentially at the active nosepoke (Fig. 6H), instead responding at equivalently low levels at both active and inactive nosepoke ports.

Next, we asked if the contingency between behavioral responses and DA ICSS was required to sustain responding. Rats were allowed to respond for stimulation over 30 minutes ("maintenance"), followed by a period of contingency degradation ("CD") during which stimulation trains were delivered pseudorandomly at intervals matched to the average rate at which they were earned by each rat during FR1-responding in a previous session. Rats could continue to respond at the active port during this phase, but the delivery of stimulation trains occurred independently of these responses. After 30 minutes had passed, non-contingent stimulation ceased and reinforcement was once again made contingent on responses in the active port ("reacquisition"). We found that *Th::Cre+* rats were sensitive to degradation of the contingency between response and reinforcement, as they performed significantly fewer active nosepokes during CD than they had during maintenance (2-tailed Wilcoxon signed rank test, $p<0.01$; Fig. 6I,J) despite the fact that the number of stimulation trains delivered did not differ across the two epochs (2-tailed Wilcoxon signed rank test, $p>0.05$, Fig. 6J). Interestingly, by the last 5 minutes of the CD phase *Th::Cre+* rats still showed a small but significant preference for responding at the active nosepoke (Fig. 6K). Additionally, on average rats increased responding at the active port during reacquisition, although when summed across the 30-minute epoch this change was not statistically significant (2-tailed Wilcoxon signed rank test, $p>0.05$; Fig. 6J). Together, the extinction and contingency degradation manipulations demonstrate that the robust maintenance of *Th::Cre+* rat responding at the active port arises from response-contingent optical stimulation of DA neurons.

Discussion

Here, we introduce a panel of the first genetically-targeted and validated recombinase-driver rat lines, and demonstrate the utility of these lines as versatile and effective tools to target opsins to genetically-defined cell types in this essential animal model. Most efforts to target genetically-defined subpopulations of neurons in rats have relied on viral strategies (Lawlor et al., 2009; Lee et al., 2010), but since compact promoters are rare and viral vectors have limited packing capacity, published attempts often result in only partial specificity for the targeted cell type (Tan et al., 2008; Nathanson et al., 2009; Wang et al., 1999). In contrast, we found that BAC Cre transgenic rats offer an attractive alternative for precise optogenetic targeting. We were able to achieve 98% and 84% specific opsin expression in DA neurons of the VTA and SN respectively, as well as 97% opsin specificity in noradrenergic neurons of the LC in *Th::Cre* rats. We also observed 92%, 98% and 97% specificity in cholinergic neurons of the medial septum, nucleus basalis, and NAc, respectively, in *Chat::Cre* rats.

These lines thus offer a powerful means to selectivity target dopaminergic, noradrenergic and cholinergic neurons in rats, providing long-sought experimental control of neuronal populations that are likely to influence a wide variety of neural and behavioral functions

(Changeux, 2010; Surmeier et al., 2009; Shen et al., 2008; Gerfen and Surmeier, 2011; Nader and LeDoux, 1999; Montague et al., 2004) in this important animal system. When combined with optogenetics, these tools now enable selective control of neuromodulatory function with exceptional temporal precision in genetically-defined subpopulations and their projections, and we expect this approach to be readily generalizable to other cell types in rats. This approach capitalizes on BAC technology that had been developed for the generation of transgenic mice (Gong et al., 2007); coupling these constructs with recent advances in pronuclear injection technology in rats (Filipiak and Saunders, 2006) results in a versatile approach that will enable targeting of a virtually unlimited array of genetically-defined cell-types of interest. Our success in achieving cell-type specific expression in rats was fundamentally related to the very large regulatory/promoter element that we employed (the BACs allowed for a regulatory region of 200–300 kB), which contrasts with the much smaller promoter regions that typically can be packaged in viruses (typically 2–5 kB promoter region, depending on the type of virus and the size of the proteins being expressed by the virus). We were able to achieve specificity for both promoters (*Th* and *Chat*), although not all founders generated offspring with highly specific expression. In fact, only 1 *Th::Cre* founder (out of 7) and 1 *Chat::Cre* founder (out of 6) resulted in a high (>90%) specificity line. Thus, a primary step in the generation of transgenic rat lines is the extensive characterization required to validate transgene specificity.

We also demonstrated the efficacy of the *Th::Cre* rats for optogenetic experiments. Specifically, we used *Th::Cre* rats to clarify the relationship between DA neuron activation and positive reinforcement, and found that brief phasic optical stimulation of dopaminergic VTA neurons was sufficient to drive vigorous ICSS. Electrical ICSS experiments have been difficult to interpret in the context of phasic DA neuron activation since electrical stimulation activates a heterogeneous and complex population of neurons (Margolis et al., 2006; Fields et al., 2007; Dobi et al., 2010; Lammel et al., 2008; Histed et al., 2009; Nair-Roberts et al. 2008; Swanson, 1982) and fails to elicit reliable DA release in well-trained animals (Garris et al., 1999; Owesson-White et al., 2008). Our studies show that phasic DA stimulation can support both the acquisition and maintenance of instrumental responding, significantly extending the recent finding that optogenetic stimulation of DA neurons can support conditioned place preference (a form of Pavlovian learning; Tsai et al., 2009).

Interestingly, our characterization of DA ICSS reveals that this behavior has much in common with electrical self-stimulation. First, rats rapidly acquire responding, with some rats responding at remarkably high rates. Second, responding scales with the duration of stimulation. Third, responding is extinguished very rapidly upon cessation of stimulation. And fourth, responding requires contingency between response and reinforcement. Although the current results do not preclude an involvement of other non-dopaminergic cell types in mediating electrical ICSS, our findings demonstrate that activation of VTA DA neurons is sufficient, and the strong parallels with electrical self-stimulation are consistent with a major role of DA neuron activation in ICSS.

To our knowledge, all previous demonstrations of optogenetic modulation of mammalian behavior have been performed in mice. The larger size of the rat brain provides both advantages and challenges for optogenetic dissection of the neural circuits underlying behavior. The advantage is that a sub-structure can be targeted in the rat with greater accuracy, while the disadvantage is that more light will be required to activate the entirety of a structure given greater size. Another fundamental and relevant difference between mice and rats is that the same axon tract will extend a significantly greater distance in rats relative to mice. For example, the projection between the VTA and the NAc will be more than twice as long in rats as mice Since the time it takes an opsin to express in axons tends to increase with the length of the projection, this fact could greatly affect the utility of rats as a system

to optogenetically stimulate terminals rather than cell bodies (an approach to further increase the specificity of cell populations targeted for optogenetic stimulation). A recent finding that rats will perform ICSS to obtain stimulation not only of the DA cell bodies in the VTA, but also of the VTA DA terminals in the NAc (unpublished data, I.W., E.S., P.J., K.D.) provides confidence in the utility of the transgenic rats for optogenetic experiments, despite greater size.

In summary, we have developed a panel of transgenic rat lines that enable a wide range of experiments probing the causal role of neuromodulatory cells in neural circuit function and behavior. The size of the rat brain is amenable to *in vivo* multi-electrode recording studies that can now take advantage of the ability to optogenetically perturb activity in these neural populations in concert with recording, with immediate implications for basic and translational neuroscience. Ultimately, the increasingly sophisticated integration of these new reagents with projection-based targeting and the rich repertoire of rat behavior may continue to deepen our understanding of the neural underpinnings of behavior.

Experimental Procedures

BAC transgenic rat production

The *Th::Cre* construct consisted of a *Cre* gene introduced immediately before the ATG of the mouse *Th* gene (BAC address RP23-350E13); the *Chat::Cre* construct consisted of a *Cre* gene introduced immediately before the ATG of the mouse *Chat* gene (BAC address RP23-246B12), as described previously (Gong et al, 2007). The BAC constructs were purified using NucleoBond® BAC 100 from ClonTech. Both BAC DNAs were verified by sequencing and by pulse field electrophoresis of a Not1 digest. They were then resuspended in microinjection buffer (10 mM Tris-HCl pH 7.5 0.1 mM EDTA 100 mM NaCl + 1 x polyamine) at a concentration of 1.0 ng/ul. The constructs were injected into the nucleus of fertilized eggs (derived from mating Long Evans rats) and transferred to pseudopregnant recipients (University of Michigan transgenic core). This procedure resulted in 7 *Th::Cre* and 6 *Chat::Cre* founder lines with transgene incorporation into the genome, as determined by *Cre* genotyping (Supplemental Experimental Procedures).

Of the initial founders, 3 *Th::Cre* founders and 3 *Chat::Cre* founders exhibited robust expression of Cre-dependent opsin virus in the VTA or MS, respectively. The breeding procedure consisted of mating Cre-positive founders or their offspring with wildtype rats from a commercial source to obtain heterozygous (as well as wildtype) offspring. The advantage of using heterozygous offspring was twofold. First, it is easier to create a large, stable colony of heterozygous animals without risking in-breeding; second, heterozygous rats are less likely than homozygous rats to exhibit unwanted side-effects of expressing the transgene since they express one wildtype chromosome. The expression profile of YFP was quantified in relationship to ChAT or TH expression for the F2 generation (or later) in these lines to allow for stabilization of the transgenes, and specificity was found to be greater than 90% for the offspring of 1 *Th::Cre* (Founder 3) and 1 *Chat::Cre* founder (Founder 5). No differences in ChR2-YFP expression profile were observed between F2s originating from the same founder.

Acute slice *in vitro* electrophysiology

Coronal slices (3253m) were obtained from adult rats (3 months or older) previously injected with virus (see supplemental experimental procedures for details). In the analysis of *in vitro* electrophysiology, listed membrane potential refers to the initial potential measured immediately after attaining whole-cell configuration. To measure the magnitude of the hyperpolarization-activated inward I_h current, cells were held at −40mV, and a 500ms

voltage step to −120mV was applied. I_h was measured as the difference between the initial capacitative response to the voltage step (usually ~20–40 ms after the beginning of the voltage step) and the final steady-state current the end of the 500ms pulse; responses greater than 115pA were classified as $I_{h/large}$. The apparent input resistance was calculated from the linear portion of the steady-state I–V curve obtained by applying 500ms hyperpolarizing current pulse steps. Action potential threshold was measured as the voltage at which the first-order derivative of the membrane potential (dV/dt) exhibited a sharp transition (typically >10mV/ms). The action potential threshold was also used to set the threshold in determining spike fidelity (% of successful action potential after various light stimulation frequencies). Peak and steady-state photocurrents were measured from a 1s light pulse in voltage-clamp mode. Series resistances were carefully monitored and recordings were not used if the series resistance changed significantly (by >20%) or reached 20 MΩ. Statistical analysis was performed with a two-tailed Student's t-test, with a level of significance set at $p < 0.05$.

In vivo optrode recording

Simultaneous optical stimulation and extracellular electrical recording were performed in anesthetized rats as described previously (Gradinaru et al., 2007). See Supplemental Experimental Procedures for details.

Fast-scan cyclic voltammetry

Coronal brain slices (300–400 μm) were prepared from adult rats previously injected with virus. A carbon fiber glass electrode was positioned in the NAc under fluorescent guidance. Voltammetric measurements were made every 100 ms by application of a triangular waveform (−0.4 V to +1.4 V, at 400 V/s) to the carbon fiber electrode vs an Ag/AgCl reference electrode. To estimate changes in DA release, background current at the electrode was subtracted from the current measured immediately following optical stimulation. Background subtracted cyclic voltammogram showed peak oxidation and reduction currents at ~650 mV and −200 mV respectively, indicating the signals were due to the detection of evoked DA release, and consistent with previous results. See Supplemental Experimental Procedures for additional details.

Behavioral subjects

15 male *Th::Cre* rats, 300–550g at the start of the experiment, were individually housed in a light-regulated (12h light/dark cycle, lights on at 07:00) colony room. Food and water were available *ad libitum* throughout the experiment. Animal husbandry and all experimental procedures were in accordance with the guidelines from the National Institutes of Health and were approved in advance by the Gallo Center Institutional Animal Care and Use Committee.

Virus injection and implantation of optical fibers

Standard stereotaxic procedures were used to infuse virus (Cre-inducible ChR2 viral construct serotyped with AAV5 or AAV10 coat proteins; see Supplemental Experimental Procedures for details) in the VTA and implant optical fibers dorsal to the VTA. All coordinates are relative to bregma in mm. Although placements varied slightly from subject to subject, behavioral data from all subjects was included; see Fig. S3 for a summary of placements and associated behavioral variability. Two small burr holes were drilled unilaterally over the VTA at the following coordinates: AP −5.4 & −6.2; ML ± 0.7. A custom-made 31 gauge infuser was used to deliver 1.0 μl of virus at two depths in each hole (DV −8.2 and −7.0, all coordinates from skull surface) for a total of 4.0 μl virus delivered unilaterally to the VTA. Each 1.0 μl of virus was infused at a speed of 0.1 μl per minute

using a syringe pump (Harvard Apparatus). The virus infuser was left in place for an additional 10 minutes following each injection before it was slowly removed. A third burr hole was drilled (AP −5.8; ML ± 0.7) for the insertion of an implantable optical fiber targeted just dorsal to the VTA (DV −7.3). The implanted fiber was made in-house with optical fiber (BFL37-300, Thorlabs) and a metal ferrule (F10061F360, Fiber Instrument Sales) and was secured to the skull surface with 5 metal screws and dental cement. The following coordinates were used to infuse virus to other target structures: locus coeruleus (AP −9.6, −10.5; ML 1.5, DV −7.75), medial septum (AP 0.5, ML 0.5, DV −6.5, −7.5), nucleus basalis (AP −1.5, ML 2.5, DV −7.0, −6.0), nucleus accumbens (AP 1.6; ML 2; DV 6 &8).

Behavioral Apparatus

Experimental sessions were conducted in operant conditioning chambers (32cm W × 32 cm L × 35 cm H; Med Associates Inc.) contained within sound-attenuating cubicles. The left panel was fitted with two nosepoke ports (5 cm from floor, separated by 18 cm), each with 3 LED lights at the rear. Prior to training sessions, rats were gently attached to patch cables made in-house with optical fiber (BFL37-200, Thorlabs) encased in a durable metal spring covering (PS95, Instech). These cables terminated with a metal ferrule connector (F10061F250, Fiber Instrument Sales) that was secured to the rats' cranial implant with a fitted ceramic sleeve (F18300SSC25, Fiber Instrument Sales), and were attached at the other end to an optical commutator (Doric Lenses). This commutator was connected via a second optical patch cable to a 100 mW DPSS 473 nm laser (OEM Laser Systems). The commutator was affixed to a counter-balanced lever arm (Med Associates) to minimize cable weight and provide lift when rats were rearing. Optical stimulation was controlled by a computer running Med PC IV (Med Associates) software, which also recorded responses at both nosepoke ports.

Behavioral Procedures

All behavioral tests were conducted >5 weeks post-surgery. The tests are described in the order in which they were performed. For all test sessions, the start of a session was indicated to the rat by the illumination of a white house light and the onset of low-volume white noise (65 dB) to mask extraneous sounds. Peak light output during photostimulation was estimated to be ~ 1.5–2 mW at the tip of the implanted fiber for each session, and ~0.45–0.6 mW/mm^2 at the targeted tissue 500 μm from the fiber tip. This peak light power was based on measuring the *average* light power for the pulsed light parameters used during experiments (20 Hz, 5 ms duration), and then correcting for the duty cycle to arrive at the peak power (in this case by dividing by 0.1). The power density estimate was based on the light transmission calculator at www.optogenetics.org/calc.

Fixed-Ratio 1 (FR1) Training—During the first training session, both active and inactive nosepoke ports were baited with a crushed cereal treat to facilitate initial investigation. Rats were given four daily sessions of two hours each in which they could respond freely at either nosepoke port. For all rats (*Th::Cre+* and *Th::Cre−*), a response at the active port resulted in the delivery of a 1 sec train of light pulses (20 Hz, 20 pulses, 5 ms duration). Concurrently, the LED lights in the recess of the active port were illuminated, providing a visible cue whenever stimulation was delivered. Responses at the active port made during the 1 sec period when the light train was being delivered were recorded but had no consequence. Responses at the inactive port were always without consequence.

Duration-Response Test—The duration-response test measured the rats' response to stimulation trains that varied systematically in length. As before, all stimulation trains consisted of pulses of 20 Hz frequency and 5 ms duration. The test was organized into 9

trials, and in each trial nosepokes at the active port were rewarded with stimulation trains of a specific length (100, 80, 60, 40, 20, 10, 5, 3, or 1 pulse/train). The first trial consisted of the longest stimulation length (100 pulses); the next trial consisted of the next longest stimulation length (80 pulses), and so on in descending order. A series of all 9 trials was considered to be a "sweep." A session consisted of four consecutive sweeps. The data presented is an average of all 8 sweeps from two consecutive days of testing. The start of a trial was signaled by the illumination of the house light and the onset of low-level white noise as described above. Three "priming" trains of stimulation were then delivered non-contingently to inform the rat of the stimulation parameters that would be available on the upcoming trial. The separation between these trains was equal to the length of stimulation or 1 second, whichever longer. Once the priming trains had finished, the subject then had the opportunity to earn up to 60 stimulation trains during that trial; this was true regardless of the length of stimulation delivered. The length of an individual trial was 60 × the length of stimulation train or 60 × 1 second, whichever longer. For stimulation lengths of 20 pulses or greater, a new stimulation train could be earned as soon as the previous train had finished. For stimulation lengths of 10 pulses or less, there was a short timeout (1 sec–length of stimulation train) before the next train could be earned. This was to ensure that it was physically possible for subjects to respond for all available trains regardless of the stimulation length used. At the end of each trial, the house light and the white noise were turned off. After an inter-trial interval of approximately 1 minute, the next trial began.

Extinction and Reacquisition—During this 1.5 hour test session subjects were initially given 30 min of regular FR1 training. Subsequently, a within-session extinction period began. During this phase, responses at the active port were recorded but had no consequence. After 30 min of extinction had elapsed, 5 stimulation trains (each train 1 sec long, inter-train interval = 1 sec) were delivered to signal the renewed availability of reinforcement at the active port. For the rest of the session rats were reinforced on an FR1 basis for responses at the active port.

Contingency Degradation—On the day before the contingency degradation test, subjects were given an additional 1 hour FR1 training session. The number of stimulation trains delivered during this session (dependent on subjects' responses at the active port) was used to calculate the average rate of stimulation for the contingency degradation portion of the experiment. The next day, rats were given 30 min of regular FR1 training. Subsequently, a within-session contingency degradation period began. During this phase, stimulation trains were delivered pseudorandomly and non-contingently at a rate that was matched to each subjects' performance during FR1 training on the previous day. After a further 30 min had elapsed, a reacquisition phase was initiated. During this phase, stimulation was once again contingent on a response made at the active port. The total length of this test was 1.5 hours. During this experiment, whenever a stimulation train was delivered (regardless of whether it had been earned by a nosepoke response or was delivered non-contingently) the LED lights in the active port were concurrently illuminated.

Data Analysis

The behavioral data was analyzed with non-parametric tests as specified (e.g. Wilcoxon signed rank rest for paired data, Mann Whitney test for unpaired data) coupled with Bonferroni tests to control for multiple comparisons where appropriate. This statistical approach resulted in a conservative measure of statistical significance. Given that the behavioral data was distributed in a non-Gaussian manner, and the different behavioral conditions varied greatly in their variance (e.g. Fig 6B), a parametric ANOVA would not have been an appropriate statistical choice for this data set. For the duration-response test (Fig. 6E), before averaging across rats, an individual rat's response rate was divided by the

response rate for the condition with the maximum responding. Since the condition that corresponded to the maximum rate was not the same for all rats, on average this resulted in a maximum normalized response rate below 1.

Supplementary Material

Refer to Web version on PubMed Central for supplementary material.

Acknowledgments

We would like to thank Caroline Bass (cebass@buffalo.edu) for generously providing ChR2-YFP virus packaged as the potent AAV10 serotype, and Nathaniel Heintz at Rockefeller University for his generous gift of the TH and ChAT BAC Cre DNA constructs. We would like to thank Inbal Goshen and Ramesh Ramakrishnan for advice and experimental assistance, as well as Stephan Lammel and Elyssa Margolis for advice on the *in vitro* VTA recordings. I.B.W. is supported by the Helen Hay Whitney Foundation; E.E.S and K.A.Z. are supported by an NSF Graduate Research Fellowship; T.J.D. is supported by a Berry postdoctoral fellowship; K.M.T is supported by NRSA fellowship F32 MH880102 and PILM (MIT). P.H.J. is supported by P50 AA017072 and R01 DA015096, and funds from the State of California for medical research on alcohol and substance abuse through UCSF. Full funding support for K.D. is listed at www.optogenetics.org/funding, and includes the Keck, Snyder, Woo, Yu, and McKnight Foundations, as well as CIRM, the DARPA REPAIR program, the Gatsby Charitable Foundation, the National Institute of Mental Health, and the National Institute on Drug Abuse.

References

Adamantidis AR, Tsai HC, Boutrel B, Zhang F, Stuber GD, Budygin EA, Touriño C, Bonci A, Deisseroth K, de Lecea L. J Neurosci. 2011; 31(30):10829–10835. [PubMed: 21795535]

Bari A, Dalley JW, Robbins TW. The application of the 5-choice serial reaction time task for the assessment of visual attentional processes and impulse control in rats. Nat Protoc. 2008; 3:759–767. [PubMed: 18451784]

Berke JD, Breck JT, Eichenbaum H. Striatal versus hippocampal representations during win-stay maze performance. J Neurophysiol. 2009; 101:1575–1587. [PubMed: 19144741]

Bielajew C, Shizgal P. Evidence implicating descending fibers in self-stimulation of the medial forebrain bundle. J Neurosci. 1986; 6:919–929. [PubMed: 3486258]

Buzsàki G, Bickford RG, Ryan LJ, Young S, Prohaska O, Mandel RJ, Gage FH. Multisite recording of brain field potentials and unit activity in freely moving rats. J Neurosci Methods. 1989; 28:209–217. [PubMed: 2755179]

Changeux JP. Nicotine addiction and nicotinic receptors: lessons from genetically modified mice. Nat Rev Neurosci. 2010; 11:389–401. [PubMed: 20485364]

Chudasama Y, Robbins TW. Dopaminergic modulation of visual attention and working memory in the rodent prefrontal cortex. Neuropsychopharmacology. 2004; 29:1628–1636. [PubMed: 15138446]

Colgin LL, Denninger T, Fyhn M, Hafting T, Bonnevie T, Jensen O, Moser MB, Moser EI. Frequency of gamma oscillations routes flow of information in the hippocampus. Nature. 2009; 462:353–357. [PubMed: 19924214]

Corbett D, Wise RA. Intracranial self-stimulation in relation to the ascending dopaminergic systems of the midbrain: a moveable electrode mapping study. Brain Res. 1980; 185:1–15. [PubMed: 7353169]

Dobi A, Margolis EB, Wang HL, Harvey BK, Morales M. Glutamatergic and nonglutamatergic neurons of the ventral tegmental area establish local synaptic contacts with dopaminergic and nondopaminergic neurons. J Neurosci. 2010; 30:218–229. [PubMed: 20053904]

Fibiger HC, LePiane FG, Jakubovic A, Phillips AG. The role of dopamine in intracranial self-stimulation of the ventral tegmental area. J Neurosci. 1987; 7:3888–3896. [PubMed: 3121802]

Fields HL, Hjelmstad GO, Margolis EB, Nicola SM. Ventral tegmental area neurons in learned appetitive behavior and positive reinforcement. Annu Rev Neurosci. 2007; 30:289–316. [PubMed: 17376009]

Filipiak WE, Saunders TL. Advances in transgenic rat production. Transgenic Res. 2006; 15:673–686. [PubMed: 17009096]

Fouriezos G, Wise RA. Pimozide-induced extinction of intracranial self-stimulation: response patterns rule out motor or performance deficits. Brain Res. 1976; 103:377–380. [PubMed: 1252926]

Gallistel CR, Gomita Y, Yadin E, Campbell KA. Forebrain origins and terminations of the medial forebrain bundle metabolically activated by rewarding stimulation or by reward-blocking doses of pimozide. J Neurosci. 1985; 5:1246–1261. [PubMed: 3873523]

Garris PA, Kilpatrick M, Bunin MA, Michael D, Walker QD, Wightman RM. Dissociation of dopamine release in the nucleus accumbens from intracranial self-stimulation. Nature. 1999; 398:67–69. [PubMed: 10078530]

Gerfen CR, Surmeier DJ. Modulation of Striatal Projection Systems by Dopamine. Annu Rev Neurosci. 2011; 2011(34):441–66. [PubMed: 21469956]

German DC, Bowden DM. Catecholamine systems as the neural substrate for intracranial self-stimulation: a hypothesis. Brain Res. 1974; 73:381–419. [PubMed: 4152089]

Gong S, Doughty M, Harbaugh CR, Cummins A, Hatten ME, Heintz N, Gerfen CR. Targeting Cre recombinase to specific neuron populations with bacterial artificial chromosome constructs. J Neurosci. 2007; 27:9817–9823. [PubMed: 17855595]

Gradinaru V, Mogri M, Thompson KR, Henderson JM, Deisseroth K. Optical deconstruction of parkinsonian neural circuitry. Science. 2009; 324:354–359. [PubMed: 19299587]

Gradinaru V, Thompson KR, Zhang F, Mogri M, Kay K, Schneider MB, Deisseroth K. Targeting and Readout Strategies for Fast Optical Neural Control In Vitro and In Vivo. The Journal of Neuroscience. 2007; 27:14231–14238. [PubMed: 18160630]

Gradinaru V, Zhang F, Ramakrishnan C, Mattis J, Prakash R, Diester I, Goshen I, Thompson KR, Deisseroth K. Molecular and cellular approaches for diversifying and extending optogenetics. Cell. 2010; 141:154–165. [PubMed: 20303157]

Gutierrez R, Simon SA, Nicolelis MAL. Licking-induced synchrony in the taste-reward circuit improves cue discrimination during learning. J Neurosci. 2010; 30:287–303. [PubMed: 20053910]

Histed MH, Bonin V, Reid RC. Direct activation of sparse, distributed populations of cortical neurons by electrical microstimulation. Neuron. 2009; 63:508–522. [PubMed: 19709632]

Jog MS, Connolly CI, Kubota Y, Iyengar DR, Garrido L, Harlan R, Graybiel AM. Tetrode technology: advances in implantable hardware, neuroimaging, and data analysis techniques. J Neurosci Methods. 2002; 117:141–152. [PubMed: 12100979]

Kravitz AV, Freeze BS, Parker PRL, Kay K, Thwin MT, Deisseroth K, Kreitzer AC. Regulation of parkinsonian motor behaviours by optogenetic control of basal ganglia circuitry. Nature. 2010; 466:622–626. [PubMed: 20613723]

Lammel S, Hetzel A, Häckel O, Jones I, Liss B, Roeper J. Unique properties of mesoprefrontal neurons within a dual mesocorticolimbic dopamine system. Neuron. 2008; 57:760–773. [PubMed: 18341995]

Lammel S, Ion DI, Roeper J, Malenka RC. Projection-Specific Modulation of Dopamine Neuron Synapses by Aversive and Rewarding Stimuli. Neuron. 2011; 70:855–862. [PubMed: 21658580]

Lawlor PA, Bland RJ, Mouravlev A, Young D, During MJ. Efficient gene delivery and selective transduction of glial cells in the mammalian brain by AAV serotypes isolated from nonhuman primates. Mol Ther. 2009; 17:1692–1702. [PubMed: 19638961]

Lee JH, Durand R, Gradinaru V, Zhang F, Goshen I, Kim DS, Fenno LE, Ramakrishnan C, Deisseroth K. Global and local fMRI signals driven by neurons defined optogenetically by type and wiring. Nature. 2010; 465:788–792. [PubMed: 20473285]

Lobo MK, Covington HE 3rd, Chaudhury D, Friedman AK, Sun H, Damez-Werno D, Dietz DM, Zaman S, Koo JW, Kennedy PJ, et al. Cell type-specific loss of BDNF signaling mimics optogenetic control of cocaine reward. Science. 2010; 330:385–390. [PubMed: 20947769]

Margolis EB, Lock H, Hjelmstad GO, Fields HL. The ventral tegmental area revisited: is there an electrophysiological marker for dopaminergic neurons? J Physiol (Lond). 2006; 577:907–924. [PubMed: 16959856]

Mogenson GJ, Takigawa M, Robertson A, Wu M. Self-stimulation of the nucleus accumbens and ventral tegmental area of tsai attenuated by microinjections of spiroperidol into the nucleus accumbens. Brain Research. 1979; 171:247–259. [PubMed: 572734]

Montague PR, Hyman SE, Cohen JD. Computational roles for dopamine in behavioural control. Nature. 2004; 431:760–767. [PubMed: 15483596]

Nader K, LeDoux JE. Inhibition of the mesoamygdala dopaminergic pathway impairs the retrieval of conditioned fear associations. Behav Neurosci. 1999; 113:891–901. [PubMed: 10571473]

Nair-Roberts RG, Chatelain-Badie SD, Benson E, White-Cooper H, Bolam JP, Ungless MA. Stereological estimates of dopaminergic, GABAergic and glutamatergic neurons in the ventral tegmental area, substantia nigra and retrorubral field in the rat. Neuroscience. 2008; 152:1024–1031. [PubMed: 18355970]

Nathanson JL, Jappelli R, Scheeff ED, Manning G, Obata K, Brenner S, Callaway EM. Short Promoters in Viral Vectors Drive Selective Expression in Mammalian Inhibitory Neurons, but do not Restrict Activity to Specific Inhibitory Cell-Types. Front Neural Circuits. 2009; 3:19. [PubMed: 19949461]

Neuhoff H, Neu A, Liss B, Roeper J. Ih Channels Contribute to the Different Functional Properties of Identified Dopaminergic Subpopulations in the Midbrain. The Journal of Neuroscience. 2002; 22:1290–1302. [PubMed: 11850457]

Olds J. Self-stimulation experiments. Science. 1963; 140:218–220. [PubMed: 13939937]

Olds J, Milner P. Positive reinforcement produced by electrical stimulation of septal area and other regions of rat brain. J Comp Physiol Psychol. 1954; 47:419–427. [PubMed: 13233369]

Olds ME, Olds J. PHARMACOLOGICAL PATTERNS IN SUBCORTICAL REINFORCEMENT BEHAVIOR. Int J Neuropharmacol. 1963; 2:309–325. [PubMed: 14119492]

Otazu GH, Tai LH, Yang Y, Zador AM. Engaging in an auditory task suppresses responses in auditory cortex. Nat Neurosci. 2009; 12:646–654. [PubMed: 19363491]

Owesson-White CA, Cheer JF, Beyene M, Carelli RM, Wightman RM. Dynamic changes in accumbens dopamine correlate with learning during intracranial self-stimulation. Proc Natl Acad Sci USA. 2008; 105:11957–11962. [PubMed: 18689678]

Pedersen CA, Ascher JA, Monroe YL, Prange AJ Jr. Oxytocin induces maternal behavior in virgin female rats. Science. 1982; 216:648–650. [PubMed: 7071605]

Phillips PEM, Stuber GD, Heien MLAV, Wightman RM, Carelli RM. Subsecond dopamine release promotes cocaine seeking. Nature. 2003; 422:614–618. [PubMed: 12687000]

Pontecorvo MJ, Sahgal A, Steckler T. Further developments in the measurement of working memory in rodents. Brain Res Cogn Brain Res. 1996; 3:205–213. [PubMed: 8806023]

Royer S, Zemelman BV, Barbic M, Losonczy A, Buzsáki G, Magee JC. Multi-array silicon probes with integrated optical fibers: light-assisted perturbation and recording of local neural circuits in the behaving animal. Eur J Neurosci. 2010; 31:2279–2291. [PubMed: 20529127]

Shen W, Flajolet M, Greengard P, Surmeier DJ. Dichotomous dopaminergic control of striatal synaptic plasticity. Science. 2008; 321:848–851. [PubMed: 18687967]

Surmeier DJ, Plotkin J, Shen W. Dopamine and synaptic plasticity in dorsal striatal circuits controlling action selection. Curr Opin Neurobiol. 2009; 19:621–628. [PubMed: 19896832]

Swanson LW. The projections of the ventral tegmental area and adjacent regions: a combined fluorescent retrograde tracer and immunofluorescence study in the rat. Brain Res Bull. 1982; 9:321–353. [PubMed: 6816390]

Tan W, Janczewski WA, Yang P, Shao XM, Callaway EM, Feldman JL. Silencing preBötzinger complex somatostatin-expressing neurons induces persistent apnea in awake rat. Nat Neurosci. 2008; 11:538–540. [PubMed: 18391943]

Tsai HC, Zhang F, Adamantidis A, Stuber GD, Bonci A, de Lecea L, Deisseroth K. Phasic firing in dopaminergic neurons is sufficient for behavioral conditioning. Science. 2009; 324:1080–1084. [PubMed: 19389999]

Tye KM, Prakash R, Kim SY, Fenno LE, Grosenick L, Zarabi H, Thompson KR, Gradinaru V, Ramakrishnan C, Deisseroth K. Amygdala circuitry mediating reversible and bidirectional control of anxiety. Nature. 2011; 471:358–362. [PubMed: 21389985]

Uchida N, Mainen ZF. Speed and accuracy of olfactory discrimination in the rat. Nat Neurosci. 2003; 6:1224–1229. [PubMed: 14566341]

Vanderschuren LJMJ, Everitt BJ. Drug seeking becomes compulsive after prolonged cocaine self-administration. Science. 2004; 305:1017–1019. [PubMed: 15310907]

Wang Y, Yu L, Geller AI. Diverse stabilities of expression in the rat brain from different cellular promoters in a helper virus-free herpes simplex virus type 1 vector system. Hum Gene Ther. 1999; 10:1763–1771. [PubMed: 10446916]

Wilson MA, McNaughton BL. Dynamics of the hippocampal ensemble code for space. Science. 1993; 261:1055–1058. [PubMed: 8351520]

Wise RA. Addictive drugs and brain stimulation reward. Annu Rev Neurosci. 1996; 19:319–340. [PubMed: 8833446]

Wise RA, Rompre PP. Brain dopamine and reward. Annu Rev Psychol. 1989; 40:191–225. [PubMed: 2648975]

Witten IB, Lin SC, Brodsky M, Prakash R, Diester I, Anikeeva P, Gradinaru V, Ramakrishnan C, Deisseroth K. Cholinergic interneurons control local circuit activity and cocaine conditioning. Science. 2010; 330:1677–1681. [PubMed: 21164015]

Yamaguchi T, Wang HL, Li X, Ng TH, Morales M. Mesocorticolimbic Glutamatergic Pathway. The Journal of Neuroscience. 2011; 31:8476–8490. [PubMed: 21653852]

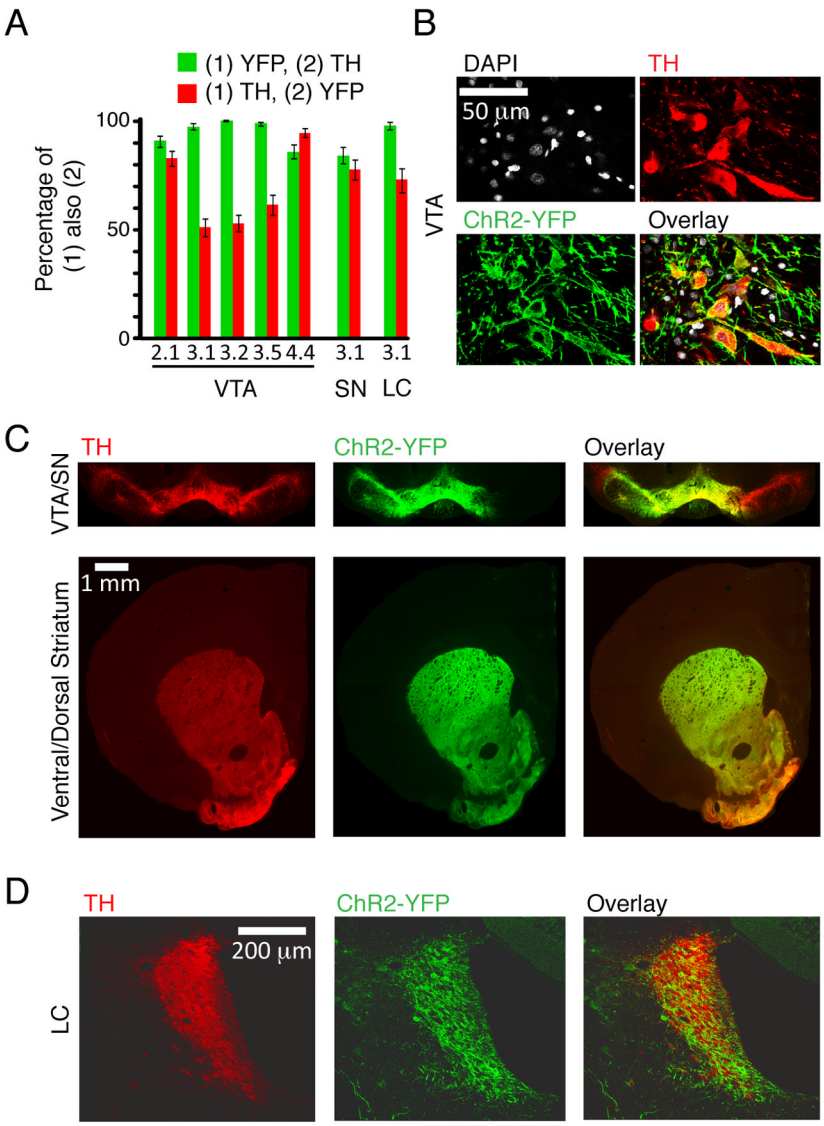

Figure 1. Specific ChR2-YFP expression in the VTA, SN, and LC of Th::Cre rats

A. Quantification of ChR2-YFP expression profile in several *Th::Cre* sublines (VTA: line 2.1 *n*=113, line 3.1 *n*=150, line 3.2 *n*=190, line 3.5 *n*=122, line 4.4 *n*=126; SN: line 3.1 *n*=86; LC: line 3.1 *n*=63 where *n* refers to the number of counted cells that expressed either YFP or TH). Error bars are SEM. **B.** High magnification view of ChR2-YFP expression and DAPI staining in TH VTA cell bodies after injection of Cre-dependent virus in the VTA of a *Th::Cre* rat. **C.** TH staining and ChR2-YFP expression in coronal slices display colocalization in cell bodies (top: VTA and SN) and efferents in the ventral and dorsal striatum (bottom) **D.** Colocalization of TH staining and ChR2-YFP expression in the LC after injection of Cre-dependent virus in a *Th::Cre* rat.

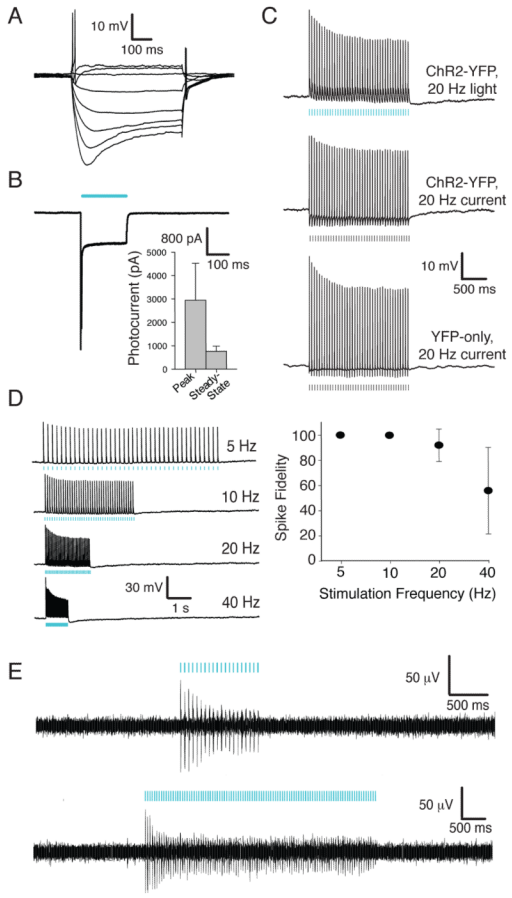

Figure 2. In vitro and in vivo physiology of optical responses in VTA DA neurons in Th::Cre rats

A. Example traces from a ChR2-expressing *Th::Cre* neuron in response to intracellular current injections (Vm: −43mV, 50pA current steps beginning at −500pA). **B.** Continuous blue light (470nm) evokes large (>500pA) inward currents in ChR2-expressing *Th::Cre* neurons. Inset, summary graph of population data for photocurrent properties (n=7). **C.** Representative responses to 20 Hz optical or electrical stimulation trains in ChR2-expressing and YFP-only expressing *Th::Cre* neurons. Spike size and shape are comparable to those previously reported for these cells. **D.** Left, ChR2-expressing *Th::Cre* neurons are able to reliably follow light-evoked pulse trains over a range of frequencies. Right, Summary data for spike fidelity (%successful spikes in 40 light flashes) in ChR2-expressing *Th::Cre* neurons (n=7; in panels **A–D** data are from $I_{h/large}$ ChR2-YFP expressing cells). Errorbars are SEM. **E.** Optically evoked time-locked multi-unit neural activity recorded with an optrode *in vivo* in the VTA of anesthetized *Th::Cre+* rats injected with Cre-dependent ChR2. Top: 20 Hz, 20 pulses, 5 ms pulse duration, 473 nm. Bottom: same recording site and photostimulation parameters but longer stimulation duration (100 pulses). Horizontal blue lines represent timecourse of optical stimulation.

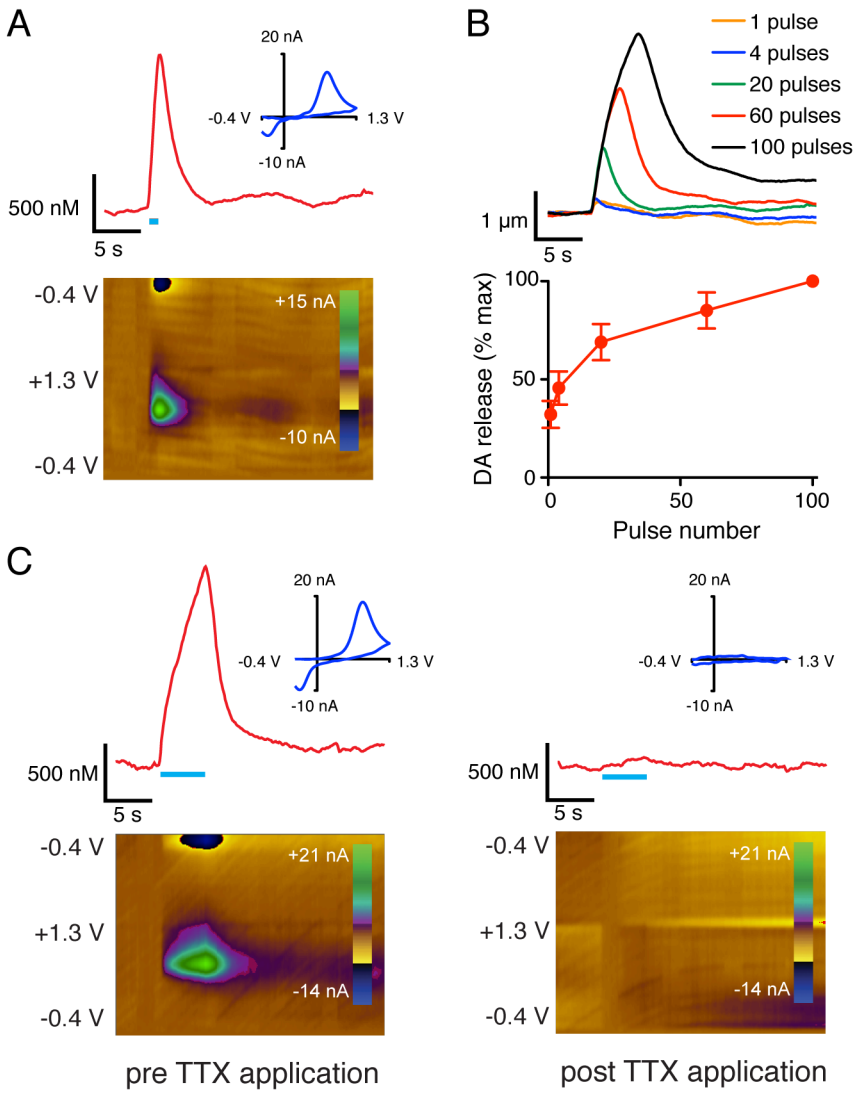

Figure 3. Voltammetric measurements of optically evoked DA release in vitro in the nucleus accumbens of Th::Cre rats expressing Cre-dependent ChR2 in the VTA

A. Timecourse of DA release at a sample site (20 pulses). **B**. Timecourse of DA release for various numbers of pulses at a sample site (top); peak DA release as a function of the number of pulses across the population (bottom, *n*=17). Errorbars are SEM. **C.** Bath application of TTX (1 uM) blocked optically-evoked DA release (left: before TTX, right: after TTX; 100 pulses. Horizontal blue lines represent timecourse of optical stimulation. In A–C, optical stimulation parameters: 20 Hz, 5 ms pulse duration, 473 nm.

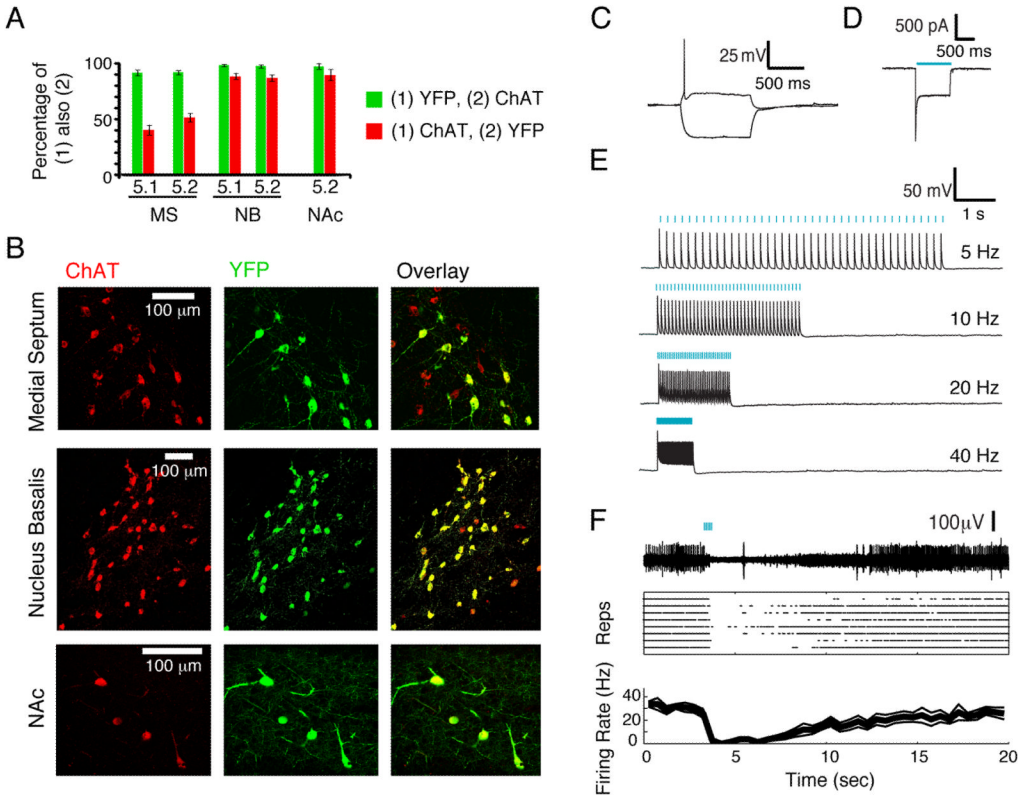

Figure 4. Specificity and functionality of Chat::Cre rats

A. Quantification of YFP expression profile in *Chat::Cre* sublines in the medial septum (MS) nucleus basalis (NB) and nucleus accumbens (NAc) after injection of a Cre-dependent virus. Errorbars are SEM. **B**. Colocalization of ChAT staining and YFP expression in the MS (top), NB (middle), and NAc (bottom). **C**. Membrane potential changes induced by current injection in a ChR2-YFP expressing ChAT neuron. VM = −53 mV. Current steps: −100, +50 pA. **D**. Voltage clamp recording of a neuron expressing ChR2-YFP in slice showing inward current in response to blue light (1 sec constant illumination, 470 nm). **E**. Current clamp recording of light-evoked action potentials in a ChAT neuron expressing ChR2-YFP in slice in response to several stimulation frequencies (470 nm, 2 ms pulse duration, 40 pulses). **F**. *In vivo* inhibition of multiunit activity in response to optical activation of ChAT cells in the nucleus basalis with ChR2. Top: example voltage trace. Middle: Raster plot from 8 repetitions. Bottom: Time average and SEM (from raster plot). (10 Hz, 10 ms pulse duration, 5 pulses, 473nm)

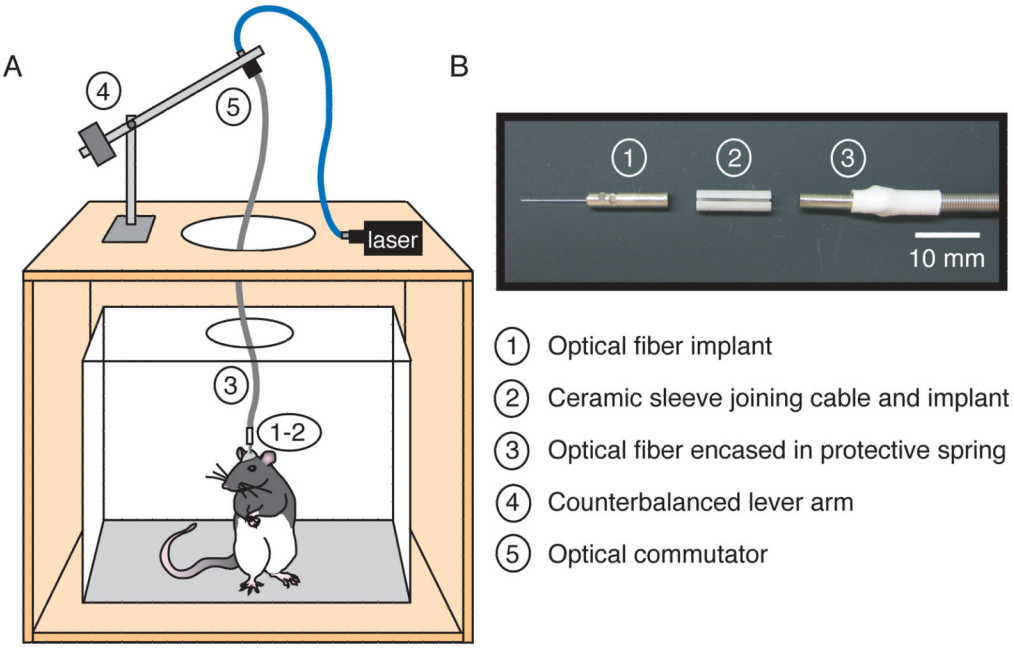

Figure 5. Rat-optimized integration of optogenetic photostimulation with freely-moving behavior in an operant conditioning chamber

A. Schematic of the behavioral set-up, which was optimized to facilitate freely-moving behavior along with photostimulation (while minimizing the chance of fiber breakage or disconnection). An optical fiber in a metal ferrule was surgically implanted over the targeted brain area (1), and connected with a ceramic sleeve (2) to a patch cable encased in a protective spring (3). A counterbalanced lever arm compensated for accumulation of slack in the patch cable during rearing (4), and an optical commutator (5) enabled the rat to rotate freely in the chamber. **B**. A close-up view of the implantable fiber in the metal ferrule (1), the ceramic sleeve (2), and the patch cord encased in the protective spring (3).

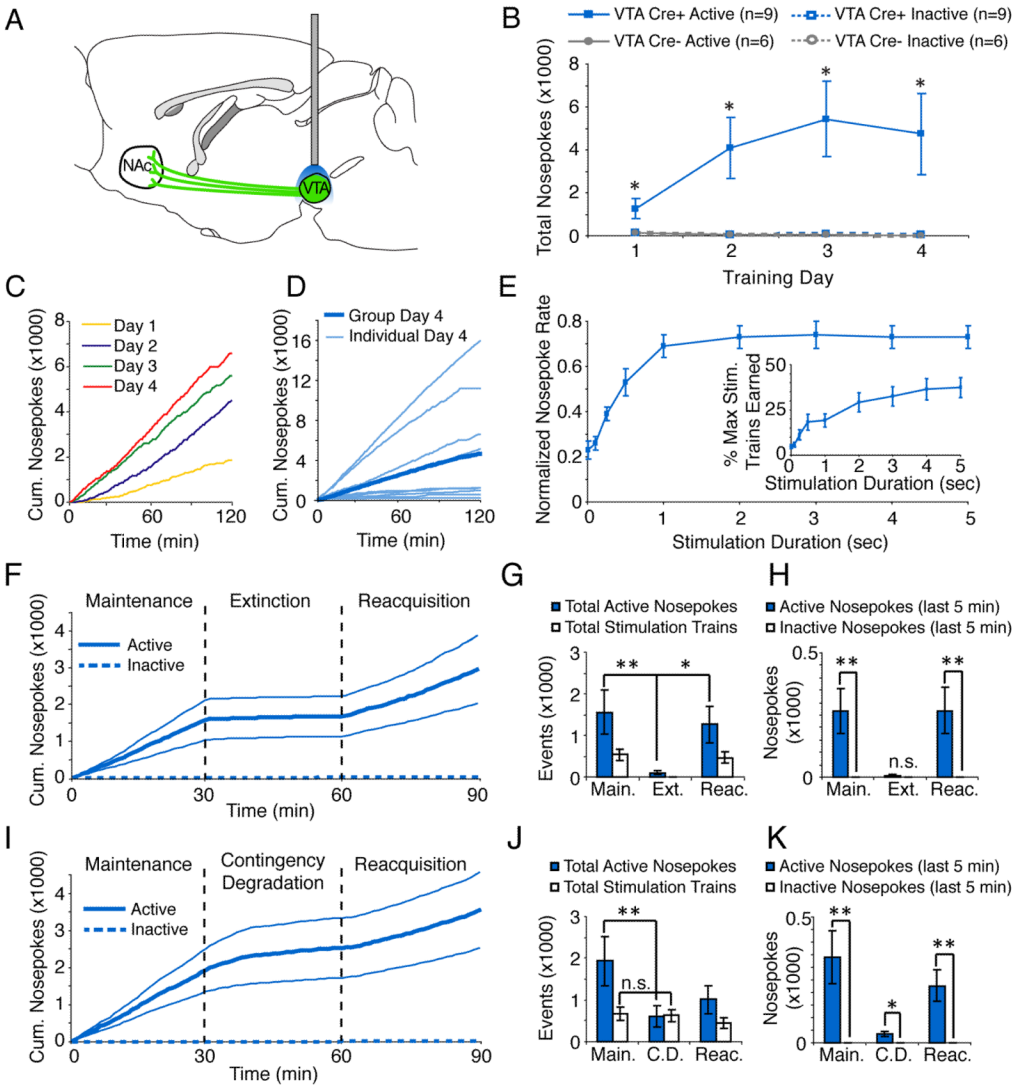

Figure 6. Optical stimulation of VTA DA neurons supports robust self-stimulation

A. The VTA was injected with a Cre-dependent ChR2 virus, and an optical fiber was implanted above the VTA. **B.** Nosepokes during 4 days of FR1 training, in which nosepokes at the active port resulted in photostimulation (20 Hz, 20 pulses, 5 ms duration, 473 nm), while nosepokes at the inactive port were without consequence. *Th::Cre+* rats performed significantly more active than inactive nosepokes (2-tailed Wilcoxon signed rank test with Bonferroni correction; $p<0.05$ on days 1–4) **C.** Cumulative responding at the active nosepoke port across all 4 days of training for a representative *Th::Cre+* rat. **D.** Cumulative responding at the active nosepoke port on Day 4 of FR1 training for all *Th::Cre+* rats. Dark blue: population average; light blue: individual rats. **E.** Normalized nosepoke rate at the active port for *Th::Cre+* rats for duration-response test in which the relationship between stimulation duration and response rate was mapped systematically. Before averaging across rats, the nosepoke rate for each rat was normalized to the maximum rate across all stimulus durations. Response rate depended on stimulation duration (Kruskal-Wallis Test, $p<0.0001$; 20 Hz, 1–100 pulses, 5 ms pulse duration). Inset: Percent of the maximum possible stimulation trains earned as a function of stimulus duration for the same data set. **F.** Cumulative responding at the active port for *Th::Cre+* rats for the within-session extinction

test during maintenance, extinction and reacquisition. **G.** Quantification of total active nosepoke responses and stimulation trains delivered during maintenance, extinction and reacquisition. Response rate decreased during extinction and then increased during reacquistion (2-tailed Wilcoxon signed rank test; $p<0.01$ for average nosepokes during maintenance vs extinction, $p<0.05$ for extinction vs reacquisition). **H.** Quantification of responses at the active and inactive nosepoke ports for the last 5 minutes of maintenance, extinction and reacquisition. *Th::Cre+* rats responded preferentially at the active nosepoke port at the end of maintenance and reacquisition, but not extinction (2-tailed Wilcoxon signed rank test; $p<0.01$). **I.** Cumulative responding at the active port for *Th::Cre+* rats for the within-session contingency degradation test during maintenance, contingency degradation and reacquisition. **J.** Quantification of total active nosepoke responses and stimulation trains delivered during maintenance, contingency degradation, and reacquisition. Response rate decreased during contingency degradation (2-tailed Wilcoxon signed rank test, $p<0.01$ for average nosepokes during maintenance vs extinction) **K.** Quantification of responses at the active and inactive nosepoke ports for the last 5 minutes of maintenance, contingency degradation and reacquisition. *Th::Cre+* rats responded preferentially at the active nosepoke port at the end of all 3 phases (2-tailed Wilcoxon signed rank test; $p<0.01$ for maintenance and reacquisition; $p<0.05$ for contingency degradation). In all panels, error bars indicate SEM.